25th ABCM International Congress of Mechanical Engineering
October 20-25, 2019, Uberlândia, MG, Brazil

COB-2019-1452
DEVELOPMENT OF A WATER FILTRATION SYSTEM FOR THE IPT TOWING TANK

Cláudio T. Rodrigues
USP - Polytechnic School of the University of São Paulo, Brazil - Av. Professor Mello Moraes, 2231- Butantã, São Paulo - SP
claudiotr@usp.br
João Lucas Dozzi Dantas
IPT - Institute for Technological Research, Brazil - Av. Prof. Almeida Prado, 532 - Butantã, São Paulo - SP
jdantas@ipt.br
Renan Santana Pelícia
USP - Polytechnic School of the University of São Paulo, Brazil - Av. Professor Mello Moraes, 2231- Butantã, São Paulo - SP
renansantanapelicia@hotmail.com
Celso Luiz Felipini
USP - Polytechnic School of the University of São Paulo, Brazil - Av. Professor Mello Moraes, 2231- Butantã, São Paulo - SP
celsofelipini@gmail.com

Abstract. *This work presents the method used to develop a water filtration system for IPTs (Institute for Technological Research, located in Sao Paulo, Brazil) Towing Tank. For the system it was decided to modify a commercial filter by replacing the filter elements for sand. For the correct sizing of the operational flow, it was studied in detail the theory of flows in porous media, determining the head loss in the sand filter through three different approaches: 1) semi-empirical formulation using the Ergun equation; 2) experimentally, through tests carried out IPTs flow laboratory; 3) Computational Fluid Dynamics (CFD). The experimental results provided validation of the model proposed by Ergun, comparing the values of pressure drop in the flow against those predicted by semi-empirical formulations and CFD. They also made possible to determine the inertial resistance* (P_i) *and viscous resistance* (P_v) *by using a quadratic adjustment of the experimental points, as well as two other important parameters: the inertial permeability* (α) *and the viscous permeability* (β) *– two of the required inputs for the CFD simulations. The analysis and visualization of current flow lines obtained from the CFD simulation allowed for a better understanding of the behavior of the flow within the porous medium, made possible to identify the recirculation regions and finally showed how the radial flow in the entrance of the filter influences the height of the filter layer. That is to say, the simulations showed that for the radial inlet the flow runs through the path of least resistance, through smaller filter layers and with less head loss, and as saturation occurs there is an increase of the filter layer along with a corresponding increase in the pressure drop.*

Keywords: *flow in porous media, filtration system, inertial and viscous resistance.*

1. INTRODUCTION

The IPTs Naval and Oceanic Engineering Laboratory has the largest towing tank in Latin America, with a water volume of approximately $7400\,\mathrm{m}^3$ (Fig. 1) and dimensions as shown in Table 1.

(a) (b)

Figure 1: (a) IPTs towing tank, (b) Water Filtration System.

Table 1: IPTs Towing Tank specifications

Dimension	Section	
	Narrow	Wide
Length	80 m	200 m
Depth	4.0 m	6.6 m
Width	2.2 m	3.5 m
Carriage Maximum velocity	3.5 m/s	

The towing tank is used to measure the resistance and maneuverability capabilities of scale ship models. The presence of suspended particles and microorganisms in the water can cause turbidity and formation of foams, which compromises the quality of photos and filming during the tests, and may also compromise the interpretation of the studied phenomena. Therefore it is necessary to develop a water filtration system to remove the solid waste precipitated in the bottom of the tank as well as the particles suspended in the surface of the water, promoting the uniformization of the physicochemical properties of water.

Figure 2 shows a schematic diagram of the operation of the water filtration system. The operation of the system begins with the suction of the water through the suction pump. The filter is distributed in the filter medium where impurities are captured by the sand and the filtered water returns to the tank.

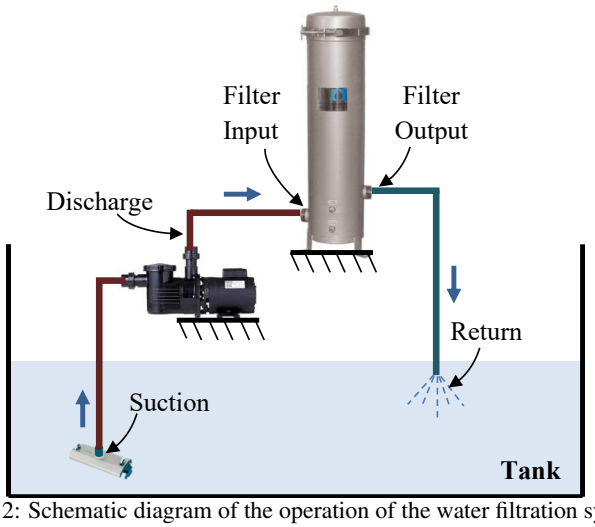

Figure 2: Schematic diagram of the operation of the water filtration system.

Figure 3 shows the modifications on the filter, wherein the filter elements (a) were removed and changes were made in the internal structure, by adding a flow uniformization chamber, and in the filtering layer body, by adding radial holes to increase the filtration rate.

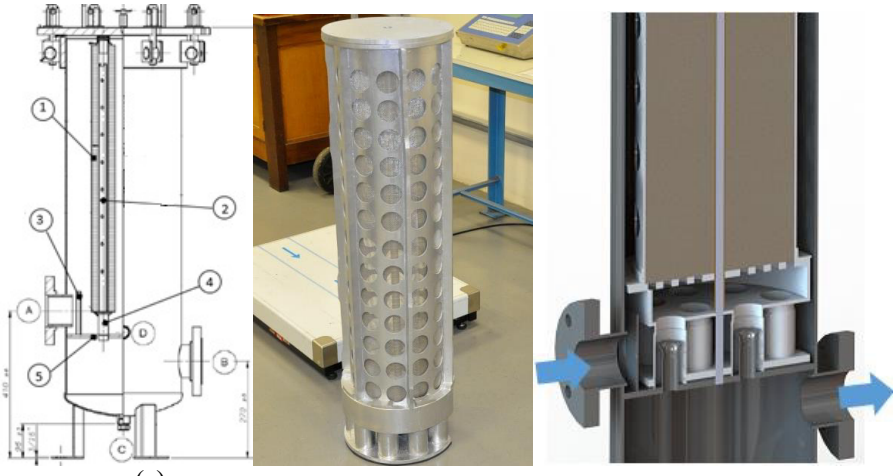

Figure 3: (a) Filter with internal filter elements before modification; (b) prototype of the modified inner structure to use sand filter layer; (c) sectional view of the internal structure installed in the filter.

2. METHODOLOGY FOR DETERMINING THE PRESSURE DROP IN THE SAND FILTER

According to Huisman and Wood (1974), filtration is a purification action in which water flows through a porous medium where the suspended material is retained. As the volume of deposited material increases, the interstitial velocity increases because of the decrease in porosity, with a corresponding increase in the pressure drop and hydrodynamic shear forces. For Di Bernardo (1980) the filtration processes are the results of two distinct mechanisms: transport and adhesion, according to Fig. 4.

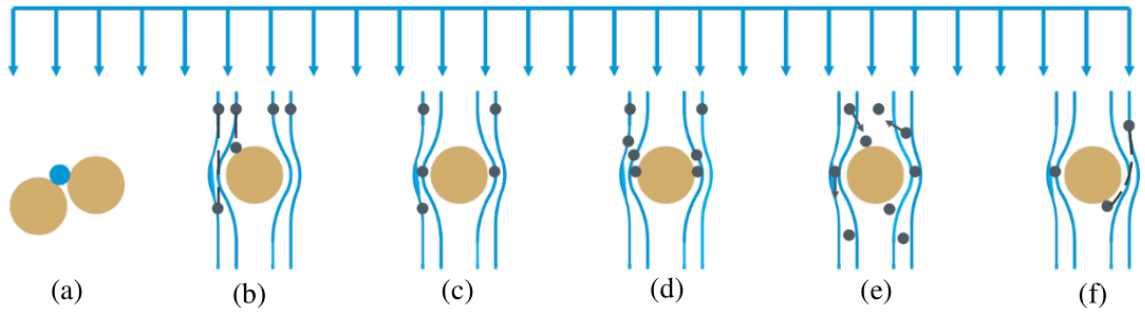

Figure 4: Mechanisms of transport and filtration of particles: coaction (a), inertial impact (b), interception (c), sedimentation (d), diffusion (e) and hydrodynamic action (f). [Figure adapted from Di Bernardo (1980)].

Through coaction (a) the particles are retained because they are larger than the granular interstices. Inertial impact (b) happens when, in the vicinity of the grains, the current lines diverge, causing particles with sufficient amount of movement to maintain their trajectory and collide with the surface of the grain. Interception (c) causes the suspended particles to be retained when the current lines are at a distance less than half the diameter of the particles. Sedimentation (d) evaluates the effect of gravity on the filtration of suspended particles. Diffusion (e) is the disordered movement of the smallest dispersed particles — on the larger particles the drag force and the inertia restrict the effects of this mechanic. And finnaly, hydrodynamic action (f) happens in the flow in which the velocity gradient is constant:the shear stress is uniform and a suspended spherical particle experiences variable tangential velocities in the direction perpendicular to the flow.

In addition to the transport mechanisms there are adhesion mechanisms that involve the electrical and van der Waals interactions. All of these mechanisms act simultaneously to a greater or lesser extent depending on the characteristics of the particulate matter and the filter medium.

Specifically for the study of pressure drop the theoretical model typically considers an axial flow through the whole height of the filter layer Trussell and Chang (1999). In the prototype constructed, however, radial holes were added with the intent of increasing the filtration rate, modifying the flow upstream from exclusively axial to partially radial. Figure 5 highlights the difference between the classical model that presumes axial flow and the expected radial flow at the inlet of the filter. Due to the different boundaries conditions it is expected that the model with radial inlets will present different results of pressure drop than those calculated by the theoretic model.

Since no applicable formulation for the radial flow case was found in the literature, it was decided to determine the values of inertial and viscous resistance through the classical mathematical model and then compare them against the values obtained through a linear regression of the collected experimental data.

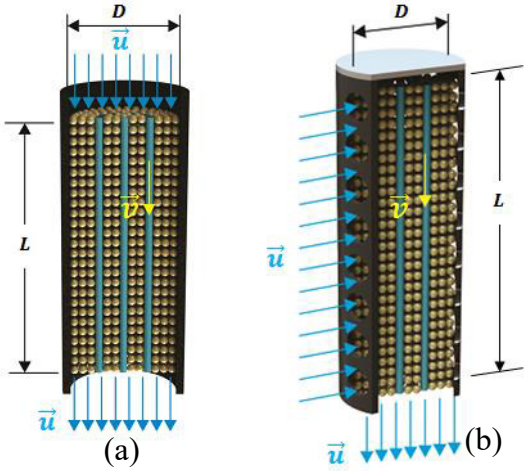

Figure 5: (a) Model with axial input; (b) Prototype with radial inlets.

2.1 Determination of the inertial resistance (P_i) and viscous resistance (P_v) using the semi-empirical model

The semi-empirical mathematical model proposed by Ergun and Orning (1949) considers that: (a) the flow is divided into bundles of tubes (Fig. 5), (b) the porosity is constant and (c) the process is in a steady state and the flow has an uniform distribution. The model is obtained from the drag force that a fluid exerts on a solid surface (Eq.1) and from a relation analogous to that of Darcy-Weisbach's (Eq.2), where v is the surface velocity; f is friction factor; f_F is Fanning friction factor; L is filter layer height, ΔP is pressure gradient, D_H is hydraulic diameter and ρ is specific mass of the fluid.

$$F_D = \frac{1}{2} f_F \rho A v^2 \tag{1}$$

$$h_l = \frac{\Delta P}{\rho} = f \frac{L v^2}{2 D_H} \tag{2}$$

The porosity (ε) is defined as the volume ratio of fluid flowing in the tubes and the total volume, and arises naturally in the definition of hydraulic diameter. Considering the sand grain a sphere, we obtain an expression for the ratio between the volumetric diameter and hydraulic diameter as a function of surface area and porosity. These expressions determine the friction factor in laminar regime as a function of porosity and surface velocity and define the permeability coefficient for linear load loss (Eq. 3). Then the friction factor for the turbulent regime is obtained and substituting the Fanning factor for 0.583 the permeability coefficient for nonlinear head loss is as follows in Eq. 4 .

$$P_v = 150 \frac{(1-\varepsilon)^2}{\varepsilon^3} \frac{\mu}{(\psi d_{sph})^2} \tag{3}$$

$$P_i = 1.75 \frac{(1-\varepsilon)}{\varepsilon^3} \frac{\rho}{(\psi d_{sph})} \tag{4}$$

If μ is dynamic viscosity, d_{sph} is diameter of the sphere and ψ is the sphericity factor of the sand, we obtain the semi-empirical model proposed by Ergun, in which the first term refers to the viscous permeability and the second term the inertial permeability. After the mathematical development of the equation, Ergun realized that there was a need to introduce an empirical constant in order to correct the considered simplifications and adjust the theoretical model with the experimental results, obtaining the following expression:

$$\frac{\Delta P}{L} = 150 \frac{(1-\varepsilon)^2}{\varepsilon^3} \frac{\mu}{(\psi d_{sph})^2} u + 1.75 \frac{(1-\varepsilon)}{\varepsilon^3} \frac{\rho}{(\psi d_{sph})} u^2 \tag{5}$$

Defining the coefficient of inertial permeability (α) as the product of inertial resistance (P_i) and filtering layer height (L) divided by the specific mass of the fluid (ρ) and defining the coefficient of viscous permeability (β) as the product of viscous resistance (P_v) and filter layer height (L) divided by the specific mass of the filter (ρ), the previous equation can be written as:

$$\frac{\Delta P}{L} = \frac{\rho}{L} \left(\alpha |V| + \beta\right) V = P_v V + P_i V^2 = 150 \frac{\mu L}{(\psi d_{sph})^2} \frac{(1-\varepsilon)^2}{\varepsilon^3} V + 1.75 \frac{\rho}{\psi d_{sph}} \frac{(1-\varepsilon)}{\varepsilon^3} V^2 \tag{6}$$

Sand with a fine granulometric fraction, sieved at a mesh aperture of 1.2 mm and granulometric composition according to ABNT (1982), was used in the Soil Mechanics Laboratory to determine the moisture content of the sand and the specific weight of the particles was determined by means of these experiments. It was possible to determine the porosity of the sand ε = 0.48, following the approach proposed by Caputo (1981).

2.2 Experimental determination the inertial resistance (P_i) and viscous resistance (P_v)

The tests were carried out at IPTs Center for Mechanical, Electrical and Fluid Flow Metrology (CTMetro), in the Fluid Flow Laboratory. The determination of the flow rates was carried according to the characteristic curves of the pump and IPTs internal procedure for the calibration of flow meters. The filter was mounted on a bench following the recommendations of ANSI / ISA-75.02-1996 - item 4.7. Figure 6 shows the experimental arrangement, where are highlighted: (1) electromagnetic flowmeter, (2) pressure transducers to measure pressure differential across the filter; (3) pressure transducer to measure the inlet pressure.

The calibration was performed according to CTMetro internal procedure CMF-SOG-PC-30, an estimation of the uncertainty in the calibration, which standards are used and the hysteresis or degree of agreement between the measurement results in a cycle is also presented. The expanded uncertainty U, which is based on a combined standard uncertainty multiplied by a coverage coefficient k, was also evaluated, providing a coverage level of 95%.

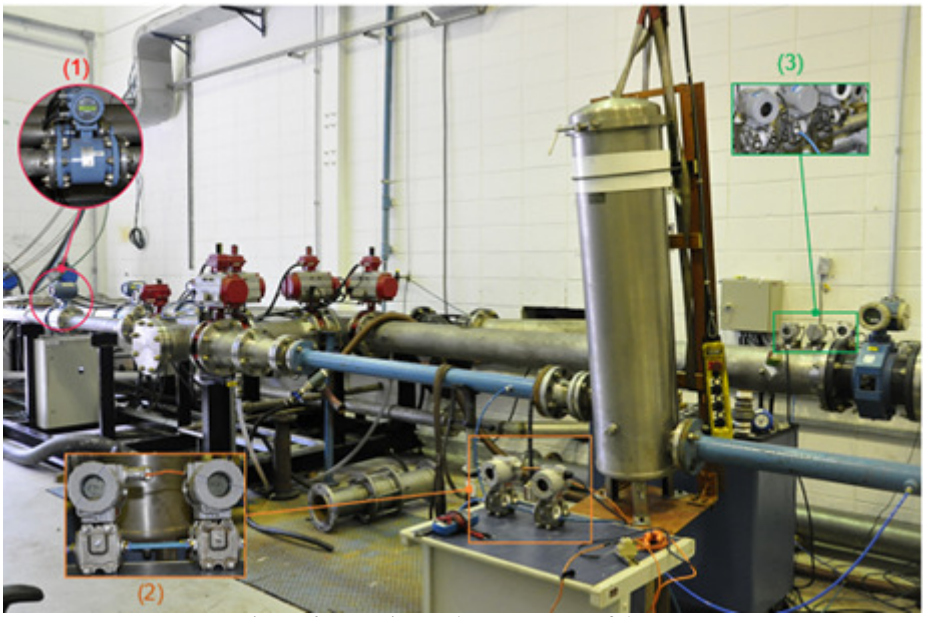

Figure 6: Experimental arrangement of the test

Eight flow rates, ranging from 65 to $10\,\mathrm{m}^3/\mathrm{h}$, were chosen according to the characteristic curve of the pump. For each flow three replications were made, waiting the necessary time for the stabilization of the flow before the acquisition of the data. The pressure differential in the filter was measured between the upstream and downstream pressure ports according to Fig. 7.

In order to obtain the values of inertial resistance and viscous resistance, the tested flows were converted from m^3/h to m^3/s, then the flow velocity was calculated in m/s by dividing the flow Q by the cross-sectional area of the filter $V = Q/A_{ST}$. After that the pressure differential measurements, in Pa, were used to plot the values of $\Delta P/L$, in N/m^3, as a function of surface velocity, V in m/s, for each flow tested and then a quadratic adjustment of the trend line of the experimental data was made.

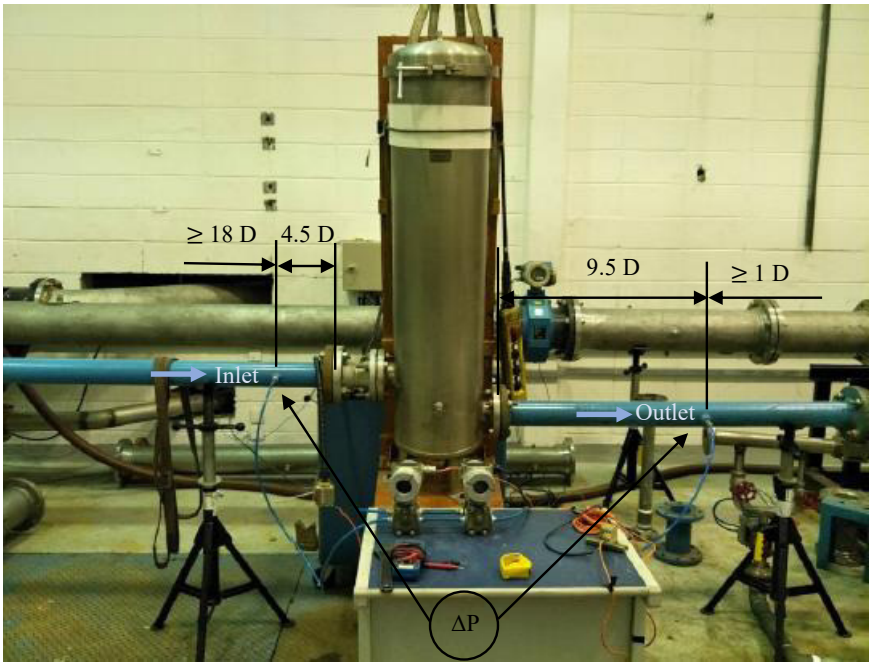

Figure 7: Filter mounting with instrumentation installed.

2.3 Numeric model

The software used on the simulations was Siemens STAR-CCM+ v12.04, which is widely used on engineering analysis of multi-physics simulation and computational fluid dynamics. Taking advantage of its reflection symmetry only half of the filter was simulated, allowing for better allocation of computational resources. In this study, an unstructured hexahedral mesh was used due to its better fitting given the complex nature of the geometry. The mesh was automatically generated using mostly trimmed cells, advantageous for their minimal cell skewness, great associated control of the transitioning of the mesh cell sizes from small to large both at the surface and far field, and finally for ease of alignment with a user specified coordinate system. To improve the accuracy of the flow solution layers of orthogonal prismatic cells were also added next to wall surfaces or boundaries. Figure 8 shows the geometry of the filter in 3D in the plane of symmetry.

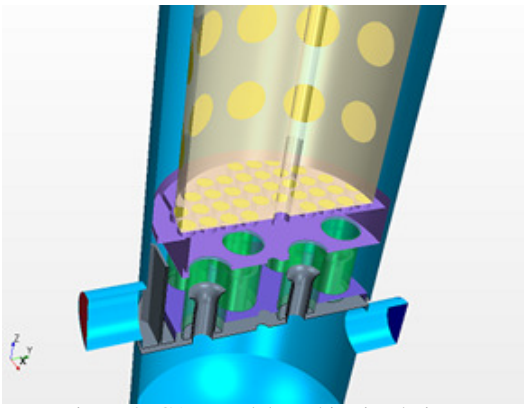

Figure 8: CAD model used in simulations

The numerical modeling of the flow was conducted solving the discrete, incompressible and steady form of the RANS (Reynolds-Average Navier-Stokes) equations, in which the pressure and velocity (momentum) transport equations are modeled using the time-average simplification, i.e., the instantaneous variables are decomposed in mean and fluctuation values. The momentum and pressure coupled equations are solved by the standard segregated method, in which each set of equations are solved individually and iteratively. The flow turbulence is modeled using the Boussinesq approach and the Reynolds stress tensor is considered homogeneous and proportional to the turbulent viscosity.

For the turbulent viscosity the Standard K-epsilon model was chosen because it is robust, have been in use for a number of decades, and it has become the most widely used model for industrial applications. It is a semi-empirical formulation that solves the transport equations for the kinetic energy k and its turbulent dissipation rate ϵ.

For the modeling of the porous medium, global variables were created that evaluate the coefficients of linear and non-linear permeability. The values assigned to them were obtained through the experimental data. The strategy for determining the pressure differential was to establish zero average output pressure as a boundary condition ($P_{out} = 0$) and allow the software to resolve what the average input pressure (P_{in}) should be.

Figure 9 shows the cross section of the volume mesh in the yz-plane after refinement at interface regions between fluid and porous medium. The transition between the volumetric mesh and the surface mesh is controlled by the prism layer's height, the number of layers inside it, the growth rate between consecutive layers and the cell base size of the volumetric mesh.

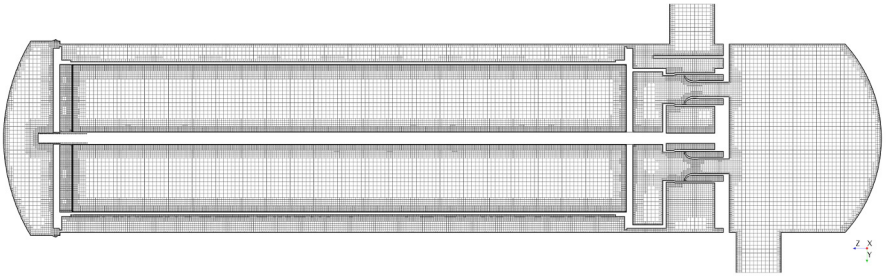

Figure 9: Filter's symmetry plane cross section of 3D mesh

3. METHOD OF OPERATIONAL DETERMINATION OF FLOW

For the determination of the operational flow, the energy conservation and mass conservation equations were applied to the control volume of Fig.10 in sections (1) to (8), using the Colebrook and White (1937).

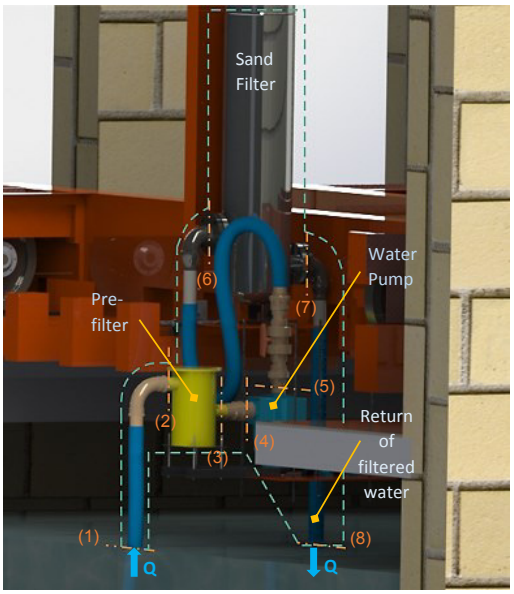

Figure 10: Control volume considered for the operational flow dimensioning.

As $H_{diss1-8}$ being the load dissipated between sections and H_{dissF} being the load dissipated in the filter, the hydrodynamic dimensioning presupposes the verification of the dynamic pressures, in order to guarantee sufficient flow and pressure, according to NBR (1994), the calculation of the distributed load loss must be performed, preferably by the Darcy-Weisbach formula.

$$\left(\frac{P_1}{\gamma}+\frac{\alpha_1\overline{V}_1^2}{2g}+z_1\right)-H_{diss1-8}+H_B-H_{dissF}=\left(\frac{P_8}{\gamma}+\frac{\alpha_8\overline{V}_8^2}{2g}\right) \tag{7}$$

The strategy used for the operational flow follows the example presented by SANTOS (2007), in which the calculation of the load dissipated in each part of the installation depends on the friction factor and the design flow rate.

$$H_B=\left[150\frac{(1-\varepsilon)^2}{\varepsilon^3}\frac{\mu L}{\rho g(\psi d_{sph})^2 A_{ST}}\right]Q+\left[1.75\frac{L}{\rho g\psi d_{sph}A_{ST}^2}\frac{(1-\varepsilon)}{\varepsilon^3}+\sum_{i=1}^{8}\left(\frac{8\sum L_{eq}}{g\pi^2 D_H^5}f\right)\right]Q^2 \tag{8}$$

The determination of the friction factor was done in an iterative manner, with the porosity value ε = 0.48 obtained experimentally, considering the coefficient of sphericity ψ = 0.85, determining the equivalent length of distributed load losses and located in each section with the hydraulic diameter , the above expression can be written as:

$$H_B=C_0Q+(C_1+C_2f)\,Q^2 \tag{9}$$

In that the coefficients C_0 and C_1 refer to the inertial and viscous resistance in the sand filter and the coefficient C_2 refers to the loss of charge in the pipes of the system, equating the expression before zero results in a complete second equation:

$$0=(C_1+C_2f)\,Q^2+C_0Q-H_B \tag{10}$$

The objective is to determine the friction factor f, but we have an equation with three unknowns, the strategy used was to estimate an average value for the pump head H_B and an initial estimate for the friction factor, the value of Q by the solution of the equation of the second degree, neglecting the negative root, after determining the Reynolds number by the Eq.12.

$$Q=\frac{-C_0+\sqrt{C^2-4(C_1+C_2f)(-H_B)}}{4(C_1+C_2f)} \tag{11}$$

$$Re=\frac{\rho D_H\overline{V}}{\mu}=\frac{4Q}{\pi D_H\nu} \tag{12}$$

A mean relative roughness value is calculated in the sections and with the Reynolds number of the flow, checks: for $Re<2300$, the flow is laminar and the Hagen-Poiseuille equation $f=64/Re$, for $2300<Re<4000$ the regime is

transitional and the friction factor is determined by the Churchill equation, for $Re > 4000$ the flow is turbulent and the calculation of the friction factor is done iteratively by the Colebrook and White formula presented by Clamond (2009):

$$\frac{1}{\sqrt{f_{n+1}}} = -2log\left(\frac{R_{rel}}{3.7} + \frac{2.51}{Re\sqrt{f_n}}\right) \tag{13}$$

Since R_{rel} is the average relative roughness, a VBA code was implemented as described by Fox *et al.* (2000), to determine the friction factor, the code replaces the repetitive queries to the Moody diagram that should be made. The value of f obtained in the iterations is replaced again in Eq.11, generating a new flow value, then calculating the Reynolds number and again with the value of the average relative roughness, we have the input parameters for the code in VBA, where a new f is obtained, the process is repeated until the difference between f_n and f_{n+1} is less than 0.1%.

After determining the value of the friction factor, it is possible to plot the characteristic curve of the installation by plotting the H_B graph as a function of the Q flow in the graph of the pump characteristic curve, the operational flow is determined at the point of intersection between the two curves.

4. RESULTS

With the experimental results of the head loss, and of the values of inertial and viscous resistance, it was noticeable that when considering the actual length of the filter layer $L = 0.9m$, and applying the mathematical model considering the axial flow at the filter inlet, the relative error observed was very expressive, that is, the values of loss of load predicted by the semi-empirical model were about five times larger than the values obtained experimentally. In this way the theoretical model was shown inconsistent with the radial flow at the entrance of the filter.

In order to understand the phenomenon of the problem, it was decided to investigate the results of the simulations. When analyzing the reports of the velocity field, it was verified that the flow was following a preferential path that offered lower resistance. According to Fig. 11 the pressures were higher on the top of the filter, forcing the flow through the porous medium initially in the lower heights of filter layer. By inference of the lines of flow of the velocity field, it was noticed that the height of the filter layer in the initial conditions was approximately $L = 0.14m$ — a length much smaller than the actual filter's length.

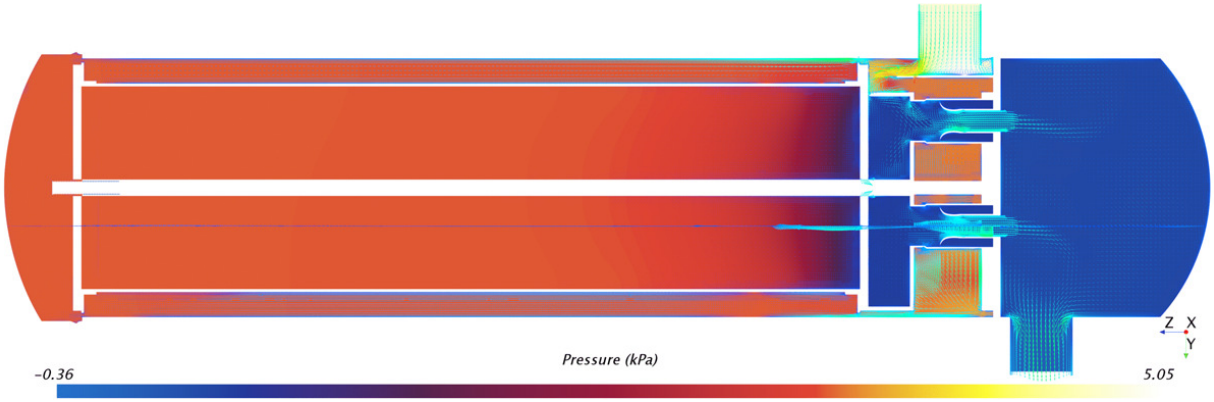

Figure 11: Pressure field showing higher pressures at the top of the filter.

Figure 12 shows that there is much recirculation of the flow in the external region of the drains below the distribution chamber. It is also possible to perceive a region of turbulence when the flow at the inlet collides with the baffle plate, after recirculation the flow flows through the walls of the filter, following an approximately spiral shape but is not able to overcome the higher pressures at the top and returns through the porous medium at heights close to $0.14m$.

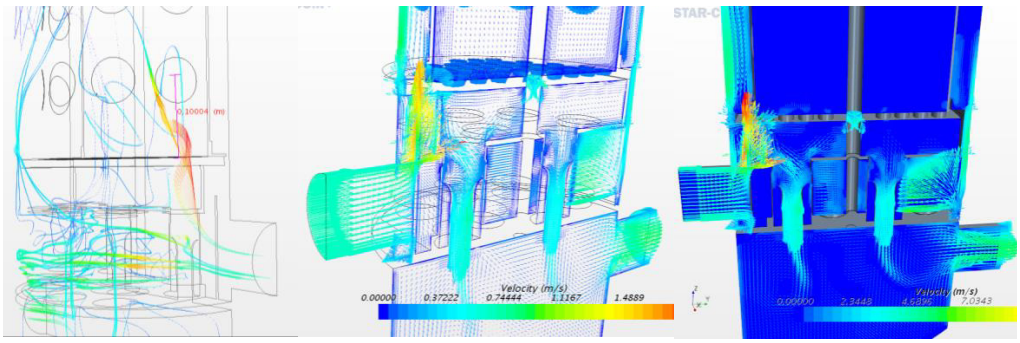

Figure 12: Visualization of the flow lines that allowed to infer the height of the filter layer.

The correction of the height of the filter layer in the semi-empirical formulation provided a considerable decrease of the relative error, making the model consistent.Table 2 shows the experimental results obtained in the IPT flow laboratory, a pressure-estimating polynomial was used: $P = A + BQ + CQ^2$, with [P] = mca and [Q] = m^3/h, A = 7.87985E-02; B = 1.03480E-02 and C = 3.38261E-03, the expanded uncertainty U was 1.69% of the estimated value, which is based on their respective combined standard uncertainty multiplied by the factor of k coverage of 2.13, assuming a 95% coverage probability, for the pressure differential measurements, the standard uncertainty was $0.22kPa$, degrees of freedom $(nieff) : 1.56e + 04$; coefficient of coverage $(k95\%) : 2.00$; Expanded uncertainty: $0.43kPa$.

Table 2: Experimental results of the test in the IPT flow laboratory

Error [%Reading]	Differential Pressure kPa	Flow Rate $[m^3/h]$	Water Temperature $[^\circ C]$	Static Pressure kPa	Atmospheric Pressure MPa	TBS $[^\circ C]$	Expanded Error[%]
-0.5	5.3 ± 0.075	10.24 ± 0.17	20.14	45.99	93.36	23.17	1.69
-1.15	16.5 ± 0.233	19.88 ± 0.34	20.27	50.80	93.33	23.25	1.69
-1.34	34.30 ± 0.484	29.91 ± 0.51	20.42	69.64	93.35	23.29	1.69
0.29	58.60 ± 0.404	39.95 ± 0.68	20.65	95.01	93.37	23.43	1.69
1.04	89.80 ± 1.149	50.14 ± 0.85	20.64	127.89	93.36	23.45	1.69
1.28	110.10 ± 1.376	55.04 ± 0.93	20.54	148.10	93.36	23.39	1.69
1.35	130.10 ± 1.834	60.16 ± 1.02	20.48	169.15	93.37	23.38	1.69
1.41	153.70 ± 2.167	65.86 ±1.11	20.38	194.14	93.38	23.32	1.69

The following Table 3 shows a comparison between the load loss values obtained by the three formulations, considering the experimental results as reference, it is noticed that the semi-empirical formulation after the correction of the height of the filter layer presented better results than those predicted by the CFD simulation, however, the views of the pressure field and the flow lines provided a better understanding of the variation of the height of the filter layer that occurs due to the radial flow at the filter inlet.

Table 3: Comparison of the analytical formulation and CFD with the experimental results

Test	Flow Rate m^3/h	Experimental ΔP [mca]	CFD ΔP [mca]	Analytical ΔP [mca]	CFD Relative Error %	Analytical Relative Error %
Q1	10.24	0.53	0.49	0.56	7.55	-5.66
Q2	19.88	1.65	1.70	1.74	-3.03	-5.45
Q3	29.91	3.43	3.74	3.64	-9.04	-6.12
Q4	39.95	5.86	6.55	6.24	-11.77	-6.48
Q5	50.14	8.98	10.23	9.57	-13.95	-6.57
Q6	55.04	11.01	12.27	11.42	-11.44	-3.72
Q7	60.16	13.01	14.61	13.54	-12.30	-4.07
Q8	65.86	15.37	17.46	16.10	-13.60	-4.75

After the determination of the pressure loss in the sand filter, it is possible to proceed in the sizing of the filtration system, to determine the friction factor in an iterative way and obtain an operational flow value as described in item 3, the results of the characteristic curve of the installation and the given operating point, are shown in the following chart.

The relative error was calculated using the experimental results as a reference, compared to the semi-empirical formulation and the CFD formulation according to the following equation:

$$Error = \frac{Value_{Experimental} - Value_{CFD,\ Analytical}}{Value_{Experimental}} x100\% \tag{14}$$

Analyzing the results it is possible to verify that the methodology proposed for the simulation was adequate, although the relative error was high for the higher flow rates, the results of the CFD simulation were able to predict with good adherence the values of loss of load obtained experimentally.

The following graph shows that the relative error of the semi-empirical or analytical formulation after adjustment of the filter layer was below 10%, which can be considered a low error, as well as the error of the CFD simulations.

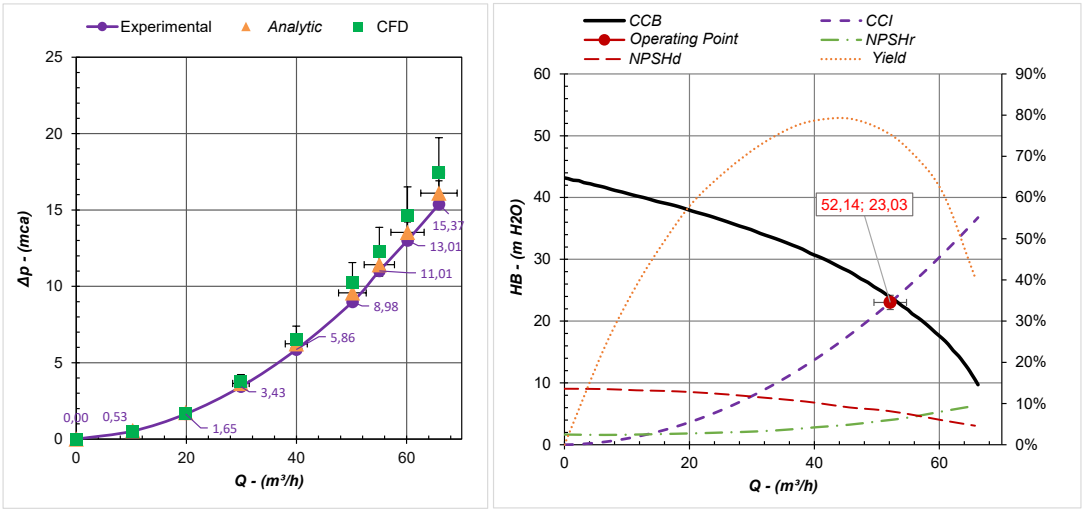

(a) (b)

Figure 13: a) Comparison of experimental results with semi-empirical formulation and CFD; b) Characteristic curves of the installation.

5. CONCLUSIONS

The CFD simulation allowed to understand the hydrodynamic behavior of the flow in the sand filter, providing a better interpretation of the experimental results from the visualizations of the vector and pressure fields and the flow lines.It was possible to evaluate the regions that had recirculation and to infer that there is a variation of the height of the filter layer as a function of the degree of saturation of the filter, that is, for the initial conditions, the flow follows the path that offers less resistance, crossing the filter also at the lower height of the filter layer.

The experimental results allowed to correctly determine the inertial and viscous resistance from the linear regression of the data, being an important entry data for the CFD simulations, and also provided the validation of the semi-empirical Ergun model. It is intended to perform transient simulations to evaluate the loss of load as a function of the variation of the height of the filter layer.

6. ACKNOWLEDGEMENTS

The authors would like to thank the technical team of the Naval Engineering and Oceance Laboratory (NAVAL) of the Institute for Technological Research for their assistance in setting up and operating the water filtration system.

7. REFERENCES

ABNT, N., 1982. "7214". *Standard sand for cement test, ABNT (Technical Standards Brazilian Association), Rio de Janeiro, Brazil*.

Caputo, H.P., 1981. "Mecânica dos solos e suas aplicações". In *Mecânica dos solos e suas aplicaçoes*, LTC.

Clamond, D., 2009. "Efficient resolution of the colebrook equation". *Industrial & Engineering Chemistry Research*, Vol. 48, No. 7, pp. 3665–3671.

Colebrook, C. and White, C., 1937. "Experiments with fluid friction in roughened pipes". *Proceedings of the Royal Society of London. Series A-Mathematical and Physical Sciences*, Vol. 161, No. 906, pp. 367–381.

Di Bernardo, L., 1980. "Teoria da filtraçao". *Revista DAE*, Vol. 40, No. 123, pp. 49–68.

Ergun, S. and Orning, A.A., 1949. "Fluid flow through randomly packed columns and fluidized beds". *Industrial & Engineering Chemistry*, Vol. 41, No. 6, pp. 1179–1184.

Fox, R.W., Pritchard, P.J. and McDonald, A.T., 2000. *Introdução À Mecânica Dos Fluidos* . Grupo Gen-LTC.

Huisman, L. and Wood, W.E., 1974. *Slow sand filtration*. Geneva: World Health Organization.

NBR, A., 1994. "12218. projeto de rede de distribuição de água para abastecimento público". *Associação Brasileira de normas Técnicas–ABNT. Rio de Janeiro*.

SANTOS, S.L.d., 2007. "Bombas & instalações hidráulicas". *São Paulo: LCTE Editora*, pp. 27–33.

Trussell, R.R. and Chang, M., 1999. "Review of flow through porous media as applied to head loss in water filters". *Journal of Environmental Engineering*, Vol. 125, No. 11, pp. 998–1006.

8. RESPONSIBILITY NOTICE

The authors are the only responsible for the printed material included in this paper.